Check for updates

Origin of Luminescent Centers and Edge States in Low-Dimensional Lead Halide Perovskites: Controversies, Challenges and Instructive Approaches

Jiming Bao[1,2,3] ✉, Viktor G. Hadjiev[4,5] ✉

✉ Jiming Bao, jbao@uh.edu; Viktor G. Hadjiev, vhadjiev@uh.edu

1. Department of Electrical and Computer Engineering, University of Houston, Houston, TX 77204, USA
2. Department of Chemistry, University of Houston, Houston, TX 77204, USA
3. Materials Science and Engineering, University of Houston, Houston, TX 77204, USA
4. Texas Center for Superconductivity, University of Houston, Houston, TX 77204, USA
5. Department of Mechanical Engineering, University of Houston, Houston, TX 77204, USA

HIGHLIGHTS

- Controversial luminescent centers and edge states in low-dimensional perovskites were summarized.

- Evaluated experimental evidences and discussed the root cause for challenges and controversies.

- New experimental techniques were suggested to resolve the controversies and identify the nature of luminescent centers.

ABSTRACT With only a few deep-level defect states having a high formation energy and dominance of shallow carrier non-trapping defects, the defect-tolerant electronic and optical properties of lead halide perovskites have made them appealing materials for high-efficiency, low-cost, solar cells and light-emitting devices. As such, recent observations of apparently deep-level and highly luminescent states in low-dimensional perovskites have attracted enormous attention as well as intensive debates. The observed green emission in 2D $CsPb_2Br_5$ and 0D Cs_4PbBr_6 poses an enigma over whether it is originated from intrinsic point defects or simply from highly luminescent $CsPbBr_3$ nanocrystals embedded in the otherwise transparent wide band gap semiconductors. The nature of deep-level edge emission in 2D Ruddlesden–Popper perovskites is also not well understood. In this mini review, the experimental evidences that support the opposing interpretations are analyzed, and challenges and root causes for the controversy are discussed. Shortcomings in the current density functional theory approaches to modeling of properties and intrinsic point defects in lead halide perovskites are also noted. Selected experimental approaches are suggested to better correlate property with structure of a material and help resolve the controversies. Understanding and identification of the origin of luminescent centers will help design and engineer perovskites for wide device applications.
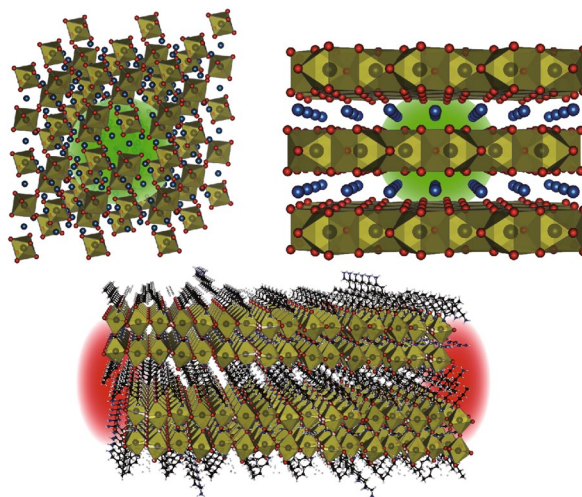
KEYWORDS Low-dimensional perovskites; Luminescent centers; Edge states; Cesium lead halides; Deep-level states; Ruddlesden–Popper perovskites

1 Introduction

Lead halide perovskites have provided us not only a long-awaited material platform to realize the dream of high-efficiency solar cells and many other optoelectronic devices, but also a wide range of structures to explore unusual fundamental sciences [1–5]. Depending on spatial configurations, lead halide octahedrons can form structures from three-dimensional (3D) all the way to 0D perovskites [6]. While still not completely understood, the superior optoelectronic properties of perovskites are believed to originate from their immunity to defects and lack of non-radiative deep-level traps, which have made them ideal materials for high-efficiency low-cost solar cells and many other optoelectronic devices [1–5, 7]. This is another reason why recent observations of possible new types of luminescent states in low-dimensional perovskites are surprising; in particular, they have been used for higher efficient solar cells and even brighter light-emitting diodes [6, 8–18]. Such apparent deep-level luminescent centers have been observed in 2D $CsPb_2Br_5$ [19–24] and 0D Cs_4PbBr_6 [11, 15, 16, 25, 26]. Because of their optical property similarities to those of $CsPbBr_3$ [27–29], the emission is believed to originate from embedded $CsPbBr_3$ nanocrystals [15, 16, 30–36]. But many other researchers attribute it to intrinsic point defects because no $CsPbBr_3$ nanocrystals have been found in their emissive samples [11, 25, 26]. The debates on the origin of Cs_4PbBr_6 are especially hot, as seen from four recent articles which acknowledge the controversy but are inclined to support one over the other [15, 16, 25, 26]. Similar deep-level luminescence centers have also been observed in low-dimensional organic–inorganic metal halide materials with better pronounced morphological dimensionality [37, 38] than that in Cs–Pb–Br system. The study of luminescence centers in structurally simpler all-inorganic lead halide perovskites, however, is expected to be instructive for further understanding the origin of these centers in all types of metal halide perovskites. As perovskites bring us more interesting properties and have found wide device applications, it is essential to understand the nature and mechanism for these luminescent centers.

In this mini review, the experimental evidences that support the opposing interpretations of the luminescence centers in Cs–Pb–Br system are analyzed, and challenges and root causes for the controversy are discussed. Selected experimental approaches are suggested to better correlate property with structure of a material and help resolve the controversies.

2 Defects and Inclusions in Cs–Pb–Br System Rooted in the Ternary Phase Diagram

The perovskite-like compounds in Cs–Pb–Br system, $CsPbBr_3$, $CsPb_2Br_5$ and Cs_4PbBr_6, can be easily synthesized via solution process or melt-grown [11, 19, 34, 39–42]. The possibility of the different phase coexistence is well expected, and the compounds are stable within narrow chemical potential ranges as shown by recent density functional theory (DFT) simulations [26].

The ternary phase diagram of the Cs–Pb–Br system shown in Fig. 1b demonstrates that the three different perovskite-like structures can be produced using only CsBr and $PbBr_2$ precursors. The different phases in Cs–Pb–Br system are grown by varying the precursor ratio (CsBr: $PbBr_2$). As shown in Ref. [43], slight change of the crystal growth conditions and controlled precursor ratios can produce the low-dimensional phases $CsPb_2Br_5$ and Cs_4PbBr_6.

The 3D perovskite $CsPbBr_3$ is the only compound in Cs–Pb–Br system that produces inherent green PL emission. This perovskite material was found unstable in moisture environment, and its instability has been used successfully to transform it into the lower dimension but stable phases $CsPb_2Br_5$ [20, 23] and Cs_4PbBr_6 [44] in water environment. The water-induced transformation of $CsPbBr_3$ into $CsPb_2Br_5$ occurs in a sequential dissolution–recrystallization process under $PbBr_2$-rich conditions [20]. Thus, synthesized $CsPb_2Br_5$ emits green photoluminescence (PL) with high PL quantum yield [20], but another approach using water was capable of growing non-emissive single crystals [23]. These observations hint that the green PL in $CsPb_2Br_5$ is likely due to highly luminescent $CsPbBr_3$ nanocrystal remnants.

Zhang et al. [44] have grown successfully a millimeter-sized Cs_4PbBr_6 bulk single crystal in concentrated CsBr aqueous solution that lacks green luminescence emission [44]. In the same work, they also demonstrate that vacuum annealing treatment activates green PL in original nongreen-luminescent Cs_4PbBr_6 crystals, which was attributed to the possible formation of $CsPbBr_3$. A reversible phase transformation between $CsPbBr_3$ and $CdPb_2Br_5$
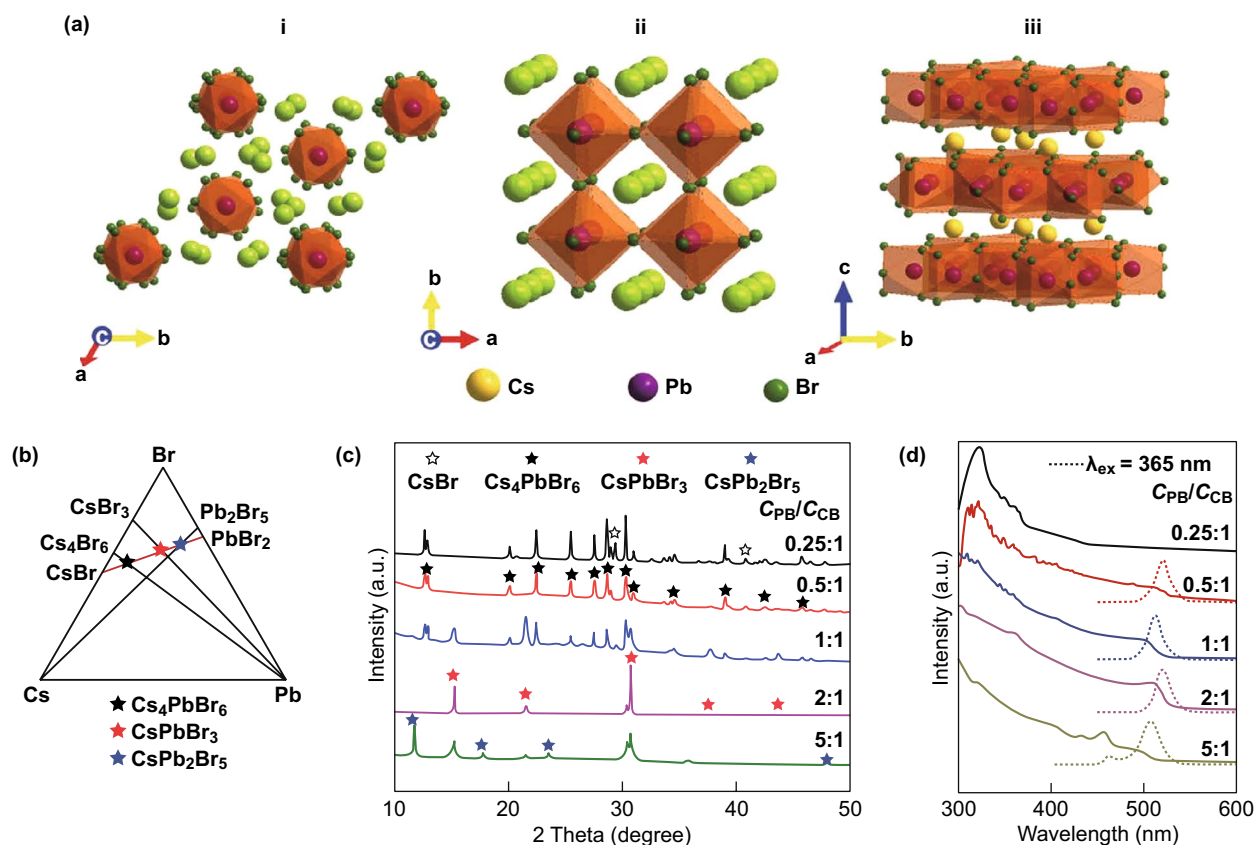
Fig. 1 Influence of C_{PB}:C_{CB} (C_{PB} = PbBr$_2$, C_{CB} = CsBr = 0.04 M) on the composition and optical properties of Cs–Pb–Br nanocrystals. **a** Crystal structure of Cs$_4$PbBr$_6$ (i), CsPbBr$_3$ (ii) and CsPb$_2$Br$_5$ (iii). **b** Ternary phase diagram of Cs, Pb and Br elements. Cs$_4$PbBr$_6$, CsPbBr$_3$ and CsPb$_2$Br$_5$ fall on the line connecting PbBr$_2$ and CsBr in the diagram. **c** XRD results at different C_{PB}:C_{CB}. **d** PL and UV–Vis absorption spectra of the nanocrystals prepared at different C_{PB}:C_{CB}. The excitation wavelength for PL spectra is 365 nm. Reprinted with permission from Ref. [43]. Copyright 2018 Royal Society of Chemistry

nanosheets under intense laser light has been demonstrated in Ref. [45]. Therefore, the narrow phase stability regions in the ternary phase diagram and the possibility of partially reversible phase transformations strongly support the expectations for foreign phase inclusions in the Cs–Pb–Br compounds.

2.1 Luminescent State in 2D Wide Bandgap CsPb$_2$Br$_5$

CsPb$_2$Br$_5$ is a layered lead halide structure with Pb-Br framework separated by Cs layers (Fig. 2a). 2D CsPb$_2$Br$_5$ has also attracted a lot of attention recently due to many conflicting reports on its luminescence although it was synthesized and studied long ago [41, 46]. Zhang et al. [21] were the first to report the beneficial effect of CsPb$_2$Br$_5$ to 3D all-inorganic perovskite CsPbBr$_3$: the attachment of

CsPb$_2$Br$_5$ nanoparticles to CsPbBr$_3$ nanocrystals enhanced PL of CsPbBr$_3$ by several folds and external quantum efficiency of CsPbBr$_3$ light-emitting diodes (LEDs) by 50%. Figure 2b, c shows that more than 90% of CsPbBr$_3$ are covered by CsPb$_2$Br$_5$ nanoparticles, but the PL and PLQY of CsPb$_2$Br$_5$/CsPbBr$_3$ are nearly the same as those of pure CsPbBr$_3$ nanocrystals. Figure 2d, e shows that these nanoparticles are not single phase, and high-resolution TEM reveals that they are CsPb$_2$Br$_5$/CsPbBr$_3$ nanocomposites with dark smaller CsPb$_2$Br$_5$ nanocrystals attached to larger CsPbBr$_3$ nanoparticles [21].

Shortly after that, Wang and co-workers reported nearly 90% quantum efficiency of pure CsPb$_2$Br$_5$ nanoplatelets and subsequently expanded their emission wavelength to whole visible spectrum using ion exchange with I and Cl [19] (Fig. 3). Note that the purity of the initial CsPb$_2$Br$_5$ and ion-exchanged nanocrystals was verified by XRD and
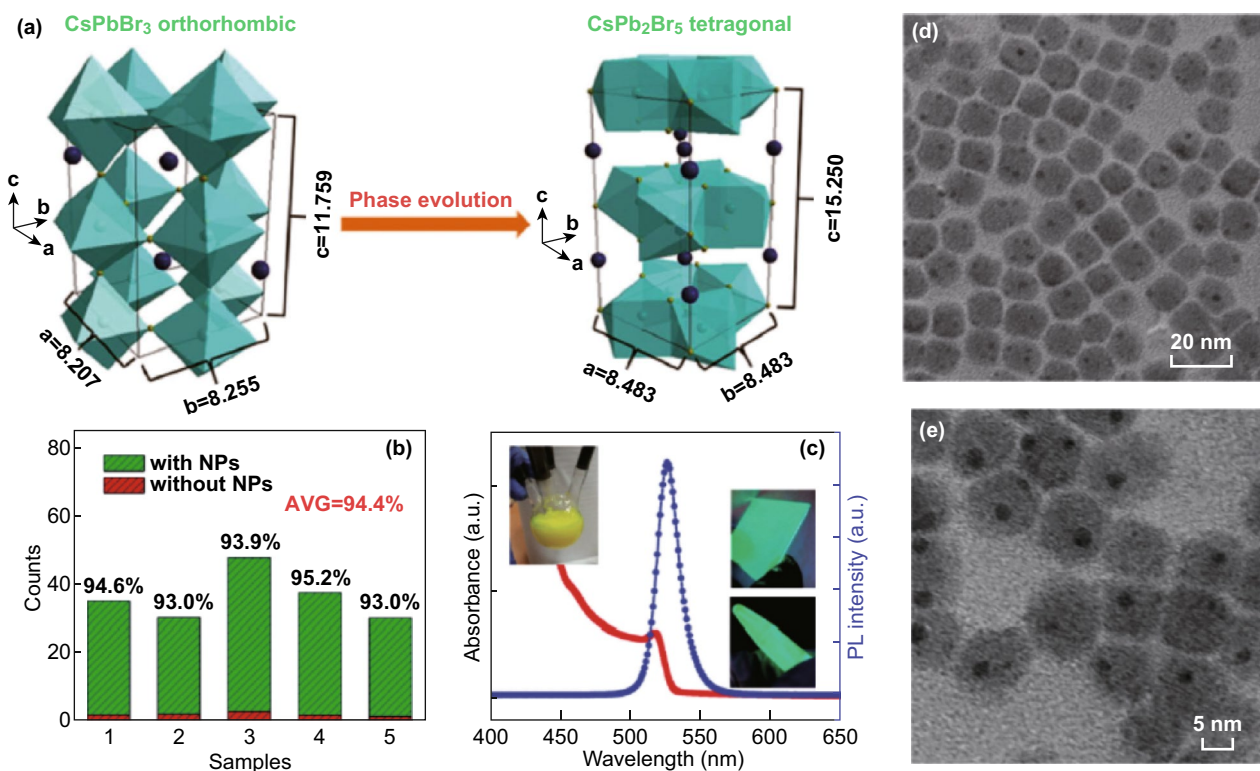
Fig. 2 a Crystal structure schematics of the orthorhombic $CsPbBr_3$ and tetragonal $CsPb_2Br_5$ (blue ball: Cs^+). The unit of all the cell parameters is Å. Reprinted with permission from Ref. [22]. Copyright 2016 Royal Society of Chemistry. **b** The percentage of the $CsPbBr_3$ nanocrystal being covered by $CsPb_2Br_5$ nanoparticles and their PL quantum yield (PLQY). **c** Absorption and PL spectra of $CsPb_2Br_5$/$CsPbBr_3$ composites. The inset shows as-obtained products in four-necked flask and light emission of $CsPb_2Br_5$/$CsPbBr_3$ deposited on the glass and tube excited with ultraviolet light. **d–e** TEM images of all-inorganic $CsPb_2Br_5$/$CsPbBr_3$ nanocomposite at different magnifications. Dark dots in **e** are $CsPb_2Br_5$ nanoparticles. Reprinted with permission from Ref. [21]. Copyright 2016 Wiley–VCH

high-resolution TEM. Since then, many groups reported strong visible photoluminescence, high-efficiency LEDs, photodetectors and even lasing action in $CsPb_2Br_5$ microplates [20, 47–54]. Highly luminescent $CsPb_2Br_5$ nanowires with mixed halides are also synthesized recently [55].

Despite numerous reports, the claim of highly luminescent $CsPb_2Br_5$ has been met with skeptics. Li et al. [22] synthesized $CsPb_2Br_5$ nanosheets from $CsPbBr_3$ nanocubes. They have found that as the reaction goes on, both absorption and PL near 520 nm disappear, and the final product of $CsPb_2Br_5$ nanosheets displays no PL at all (Fig. 4). They also performed DFT simulation. The results (Fig. 4c, d) agree with the observation that $CsPb_2Br_5$ is an indirect wide band gap semiconductor [22].

The non-emissive nature of $CsPb_2Br_5$ can be best verified from transparent large-sized sheets in Fig. 5a, b [12, 13]. Emissive macro- or micro-$CsPb_2Br_5$ typically exhibits a characteristic yellow color as shown in Fig. 3a. Different

colors of $CsPb_2Br_5$ sheets in Fig. 5b are due to their thickness-dependent optical interference under ambient or white light. As $CsPb_2Br_5$ can be produced by converting $CsPbBr_3$ particles, $CsPbBr_3$ particles can be recovered from $CsPb_2Br_5$ as well. Figure 5c shows the evolution of XRD patterns when high-purity $CsPb_2Br_5$ (black) was annealed at 220 °C (red) and 400 °C (blue). As the annealing temperature increases, X-ray pattern of $CsPbBr_3$ particles begins to appear. This observation is also confirmed by TEM. Figure 5d, e shows $CsPbBr_3$ particles attached on $CsPb_2Br_5$ in sample annealed at 400 °C. The change can also be seen in the PL spectra. The redshift of the PL band with annealing temperature is due to increasing size of $CsPbBr_3$ particles [14]. Clearly, embedded $CsPbBr_3$ particles in $CsPb_2Br_5$ can be a source for green PL emission in otherwise non-emissive pure $CsPb_2Br_5$. However, the same group has changed their mind and considered green emission as an intrinsic property of $CsPb_2Br_5$ after synthesizing
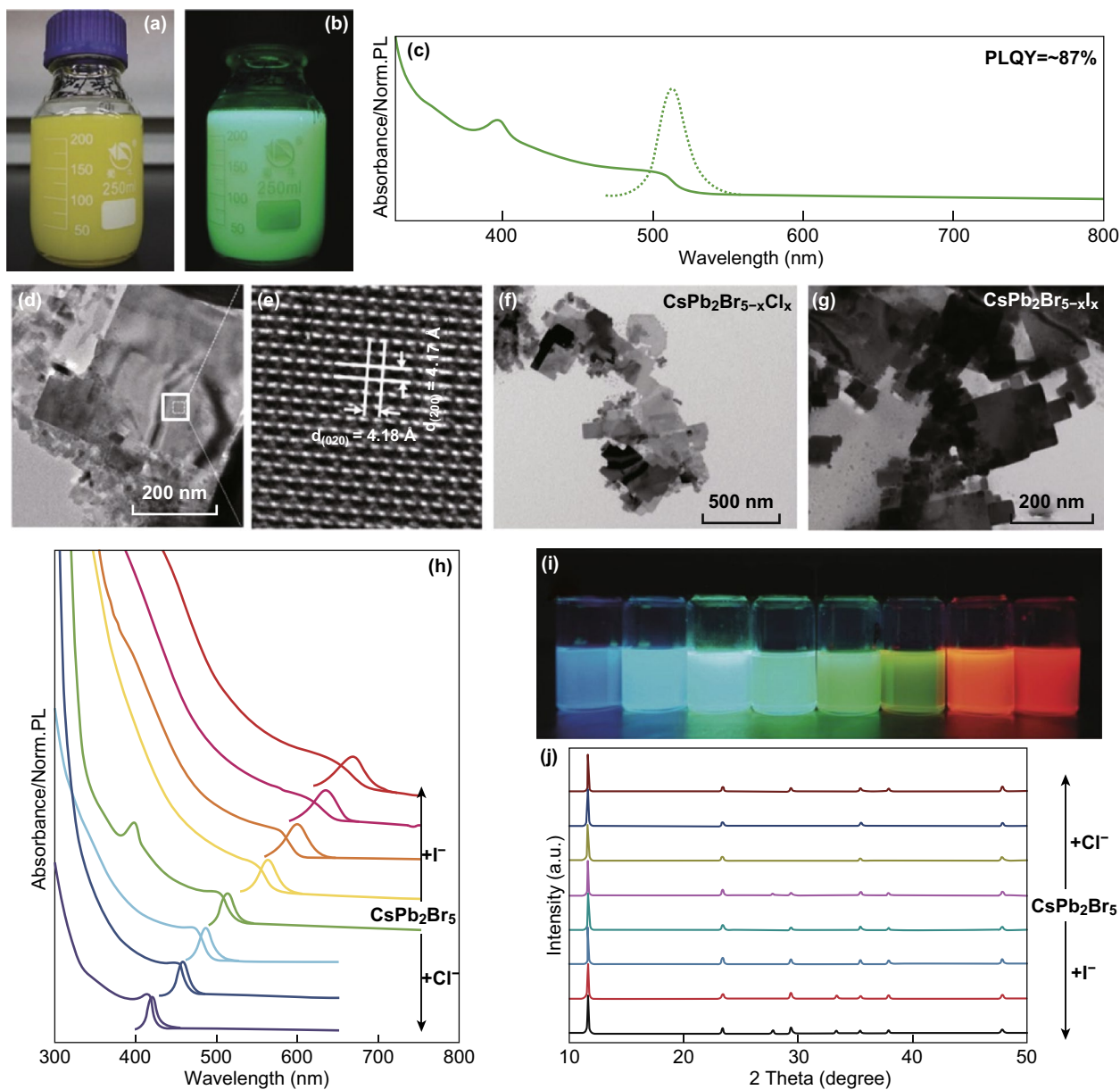
Fig. 3 **a**, **b** Photographs of as-obtained colloidal $CsPb_2Br_5$ nanoplatelets suspension under ambient conditions and the UV light (365 nm) irradiation, respectively. **c** Absorption and PL spectrum of $CsPb_2Br_5$ nanoplatelets in toluene solution. **d**, **e** TEM and HRTEM images of $CsPb_2Br_5$ nanoplatelets, respectively. **f**, **g** TEM images of representative nanostructures of $CsPb_2Br_{5-x}Cl_x$ and $CsPb_2Br_{5-x}I_x$, respectively. **h** Evolution of the optical absorption and PL spectra of $CsPb_2Br_5$ nanoplatelets with increasing quantities of anion exchange of I^- and Cl^-, respectively. **i**, **j** Corresponding photographs and powder XRD of the parent $CsPb_2Br_5$ nanoplatelet and anion-exchanged samples. Reprinted with permission from Ref. [19]. Copyright 2016 Wiley–VCH

and analyzing green emissive $CsPb_2Br_5$. Due to this reason, the mechanism for the green emission in $CsPb_2Br_5$ remains controversial. Many groups are aware of this controversy but are not able to support either of these two opposing claims [56–58].

2.2 Luminescent State in 0D Wide Bandgap Cs_4PbBr_6 Perovskite

In Cs_4PbBr_6, $PbBr_6$ octahedrons are isolated by surrounding Cs ions and each octahedron behaves as a single molecular quantum dot (Fig. 6a inset), so Cs_4PbBr_6 is called 0D
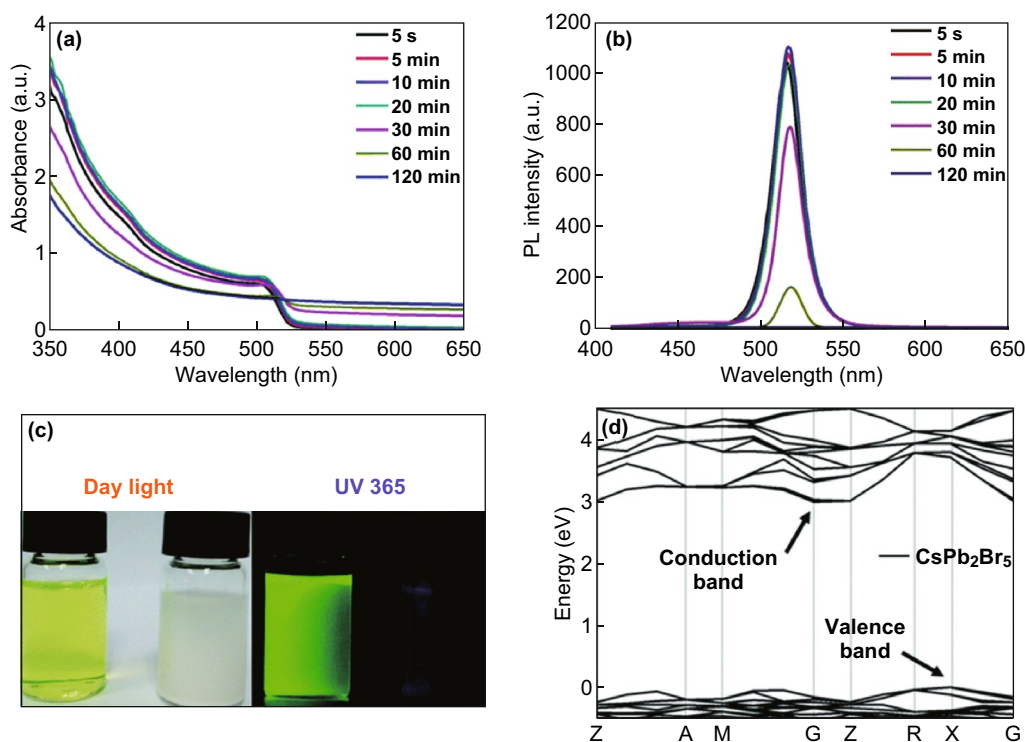
Fig. 4 Synthesis of non-emissive $CsPb_2Br_5$ nanosheets from $CsPbBr_3$ nanocubes. **a, b** Disappearance of absorbance and PL as the reaction time increases. **c** $CsPbBr_3$ nanocube solution (after 5 s reaction time) and $CsPb_2Br_5$ nanosheet suspension (after 2 h reaction time) in toluene under daylight (left) and a UV lamp (365 nm, right). **d** Calculated electronic band structure of $CsPb_2Br_5$. Reprinted with permission from Ref. [22]. Copyright Royal Society of Chemistry

perovskite [15]. On the other hand, the crystallization of Cs_4PbBr_6 in a structure with translational symmetry and fixed orientation of $PbBr_6$ octahedrons to each other clearly indicate that the spacing between $PbBr_6$ is not enough to completely deactivate the interaction between them [16]. These interactions are better suppressed in the organic 0D metal halide hybrids [59, 60], which are closer to a quantum dot material. DFT calculations of an isolated Cs_4PbBr_6 structure, however, yield an energy gap close to those of bulk Cs_4PbBr_6 [61], which justifies the assignment of Cs_4PbBr_6 to 0D materials. Specifically, Cs_4PbBr_6 has attracted a lot of attention because of the high PL quantum efficiency reported in Ref. [11]. Figure 6 shows that Cs_4PbBr_6 also emits green light with a wavelength very close to that of $CsPbBr_3$, but the PLQY is more than two orders of magnitude larger. Because Cs_4PbBr_6 is purified by dissolving $CsPbBr_3$ contamination using dimethyl sulfoxide (DMSO), and no X-ray of $CsPbBr_3$ is detected, the green emission is considered as an intrinsic property of Cs_4PbBr_6 [11]. Such strong green emission was initially attributed to the high exciton binding energy in

isolated $PbBr_6$ [11]. Later, an alternative explanation suggests that the green emission is due to a phonon-assisted transfer of photoexcited electrons to a charge-transfer state of Pb ions in the host lattice distorted by atomic displacements involved in the phonon [62]. Recently, the group published a series of papers and attributed the PL to intrinsic Br vacancies [26, 62–65]. Their theory has been supported by DFT calculations [26, 63] and other groups [25, 66–69].

The claim that the green PL emission is an intrinsic property of Cs_4PbBr_6 is also supported by the synthesis of large-sized single crystals (Fig. 7a, b). However, many other researchers do not agree with their observations and explanation [30–32, 44, 71]. Because the emission wavelength overlaps with that of $CsPbBr_3$ very well, it has been believed that the strong PL originates from embedded $CsPbBr_3$ nanocrystals. This alternative idea of non-intrinsic luminescent property is supported by the synthesis of non-emissive Cs_4PbBr_6, both large-sized single crystals (Fig. 7c) and nanocrystals [30, 44, 62, 71]. Opposing simulations also show that the Br vacancies cannot produce such deep-level defect states [5,
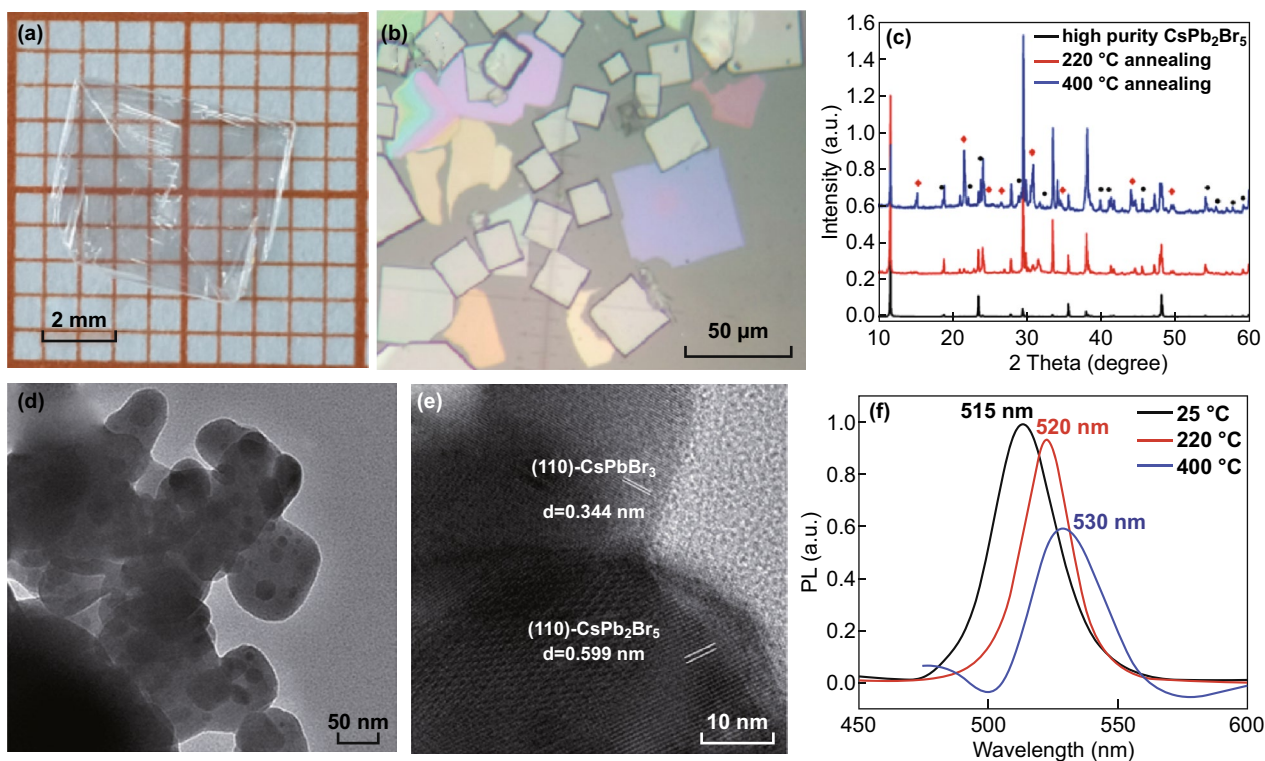
Fig. 5 **a** A transparent colorless $CsPb_2Br_5$ crystal with an area of up to 5×5 mm^2. **b** $CsPb_2Br_5$ flakes on sapphire. The thickness of the purple crystal is only 160 nm [13]. **c** Powder XRD pattern of $CsPb_2Br_5$ particles after annealing at different temperatures (red squares represent $CsPbBr_3$ (PDF#18-0364), black dots represent $PbBr_2$). **d** Low-resolution and **e** high-resolution TEM image of a representative $CsPb_2Br_5$ cluster after annealing at 400 °C. **f** PL spectra of the three $CsPb_2Br_5$ samples characterized by XRD in **c** under 400 nm excitation [14]. Reprinted with permission from Refs. [13, 14]. Copyright 2017–2018 Royal Society of Chemistry
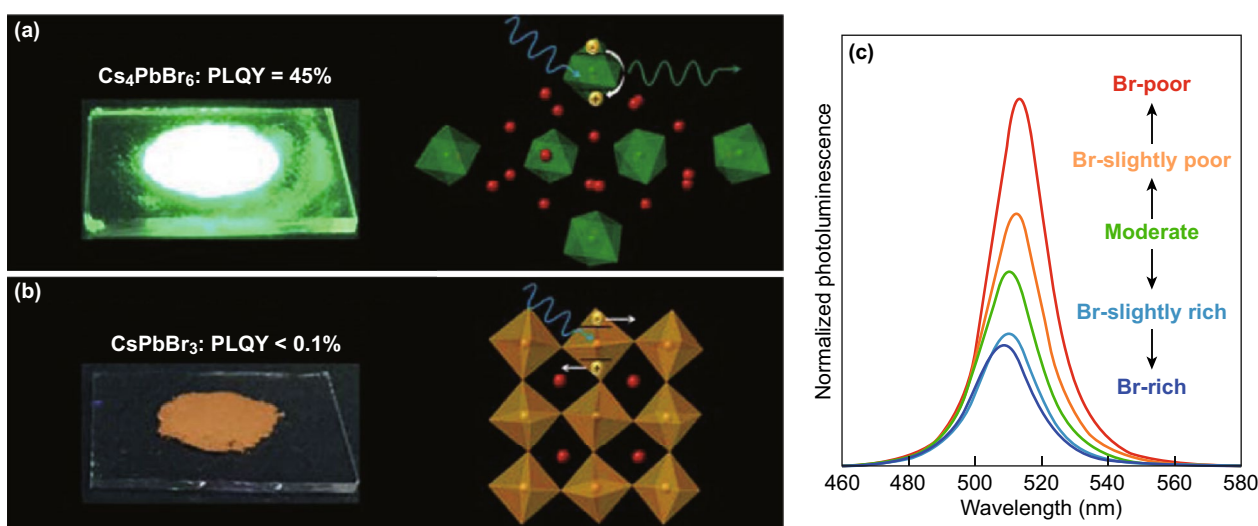

Fig. 6 **a**, **b** $CsPbBr_3$ and Cs_4PbBr_6 powders on the glass slides under UV light (365 nm). Insets are schematics of their crystal structures [11]. **c** PL intensity as a function of excitation wavelengths for Cs_4PbBr_6 (normalized PL spectra according to the absorbance at an excitation wavelength of 375 nm) [26]. Reprinted with permission from Refs. [11, 26]. Copyright American Chemical Society
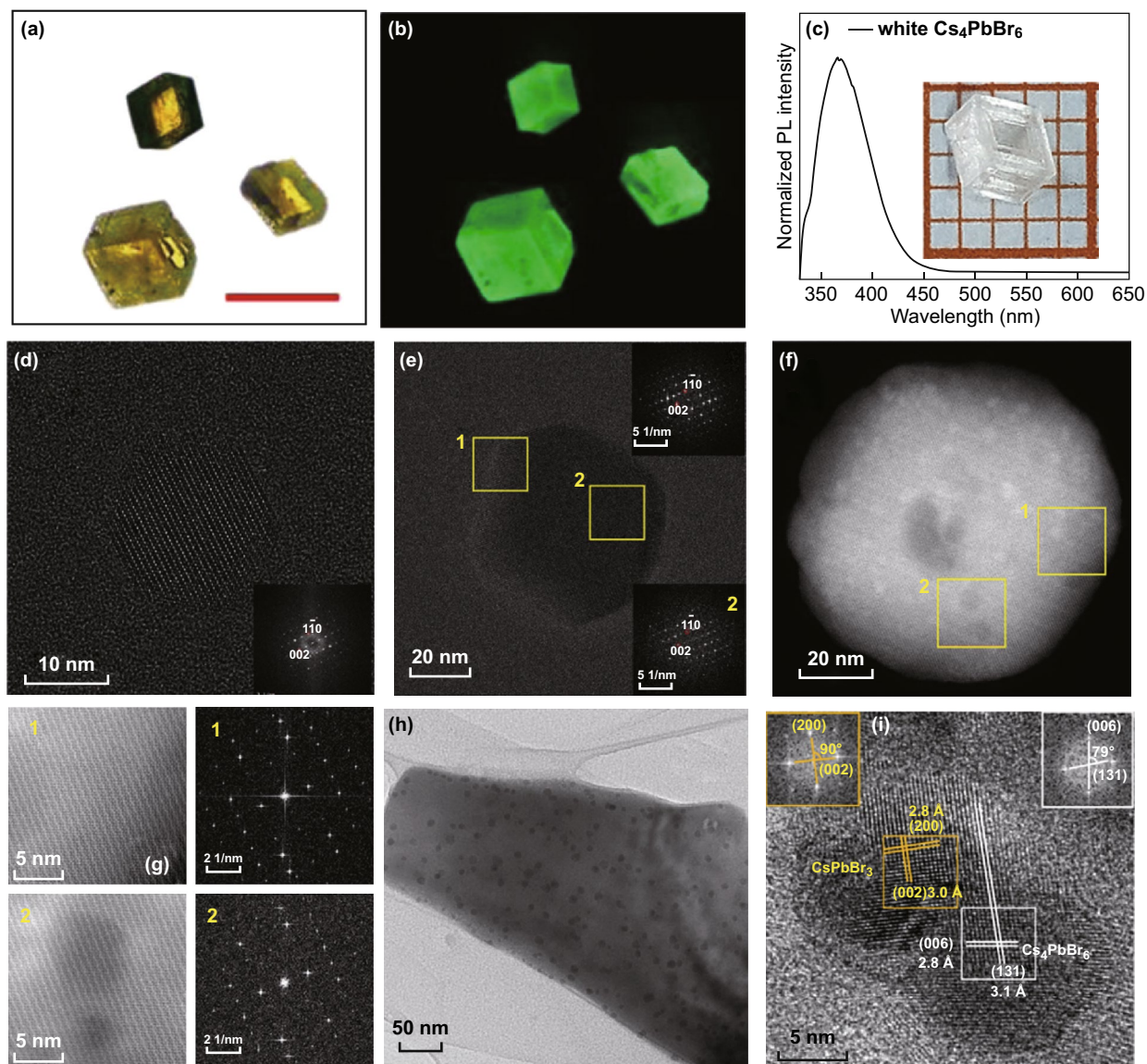
Fig. 7 **a**, **b** Optical and fluorescent microscope pictures of emissive Cs_4PbBr_6 single crystals. Scale bar: 500 μm [63]. **c** Photograph of a millimeter-sized non-emissive Cs_4PbBr_6 single crystal. Inset: PL spectrum [44]. **d**–**g** Drift-corrected HRTEM images of **d** a non-emissive and **e** a green emissive Cs_4PbBr_6 nanocrystals. The FFT patterns are shown as insets. **f** High-angle annular dark field (HAADF)-STEM image of a green emissive Cs_4PbBr_6 nanocrystal and **g** HAADF-STEM images and FFT patterns of selected areas 1 and 2 in **f** [26]. **h** TEM and **i** HRTEM images of $CsPbBr_3$ nanocrystals in the Cs_4PbBr_6 matrix. The insets show the FFT images [70]. Reprinted with permission from Refs. [26, 44, 63, 70]. Copyright American Chemical Society

15, 16, 33]. As the strongest experimental evidences, both sides show high-resolution TEM images. Figure 7d–g compares TEM images of emissive and non-emissive Cs_4PbBr_6 nanocrystals. Both types of nanocrystals exhibit clean single crystal structure, and no $CsPbBr_3$ inclusion is found. On the other hand, $CsPbBr_3/Cs_4PbBr_6$ nanocomposites have been frequently synthesized and observed, and they exhibit strong PLQY as expected [16, 34, 70, 72].

2.3 Bright Edge States in 2D Ruddlesden–Popper (R–P) Perovskites

Corner-sharing $PbBr_6$ octahedrons as those in $CsPbBr_3$ are definitely the structures that can produce visible PL. This has also been confirmed by the PL properties of two-dimensional (2D) R–P lead halide perovskites [10]. The observed

crystal edge bright PL emission, different from that of the bulk one, in these materials is very instructive with demonstrated effects of $PbBr_6$ framework relaxation at the surface of perovskite crystals.

A surface is an inevitable termination of periodic lattices of any single crystals even when we are only interested in their bulk properties. For 2D materials, edges will become surfaces and introduce surface defects as they terminate their 2D expansion. A surface will typically introduce detrimental or unwanted effects to the bulk materials so that surface treatment or passivation is crucial for the desired function or performance of materials. Because of this reason, it was very surprising that the edges of 2D organic–inorganic perovskites provide a deep-level luminescent center that also enhances the performance of solar cells [10].

In 2017, Blancon et al. [10] reported that 2D R–P perovskites $(BA)_2(MA)_{n-1}Pb_nI_{3n+1}$ exhibit a low energy photoluminescence in the edge of exfoliated flakes when n is 3 or larger (Fig. 8a–c). Their emission energy is ~ 300 meV below the band gap of $(BA)_2(MA)_{n-1}Pb_nI_{3n+1}$. Unlike conventional deep-level defect states, they can quickly dissociate photoexcited excitons and prevent electron–hole from non-radiative recombination [10]. By fabricating 2D platelets vertically and having edges directly connected to the electrodes, the
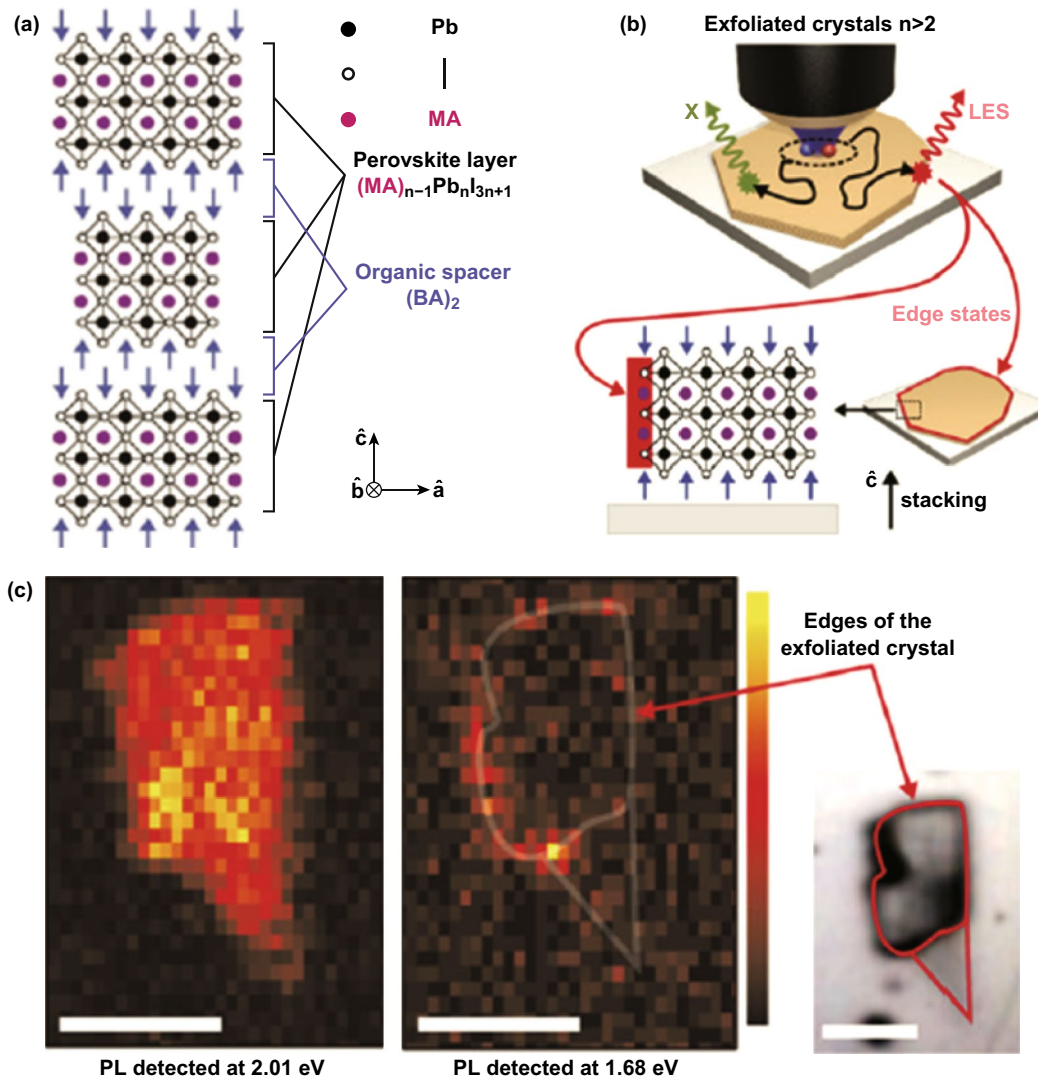

Fig. 8 Edge emission in $(BA)_2(MA)_{n-1}Pb_nI_{3n+1}$ 2D R–P perovskite with $n = 3$. **a** Schematics of crystal structure. **b** Schematics of the photoabsorption and PL processes in 2D perovskite exfoliated crystals with $n > 2$. **c** Photoluminescence intensity map of a single exfoliated crystal. Scale bar is 10 μm. Reprinted with permission from Ref. [10]. Copyright American Association for the Advancement of Science

researchers have demonstrated 12% efficiency of 2D perovskite cells [10]. However, the nature of the edge states was not totally understood, and even their chemical composition and microscopic structure have not been experimentally identified in their initial report [10].

It was not until a year later that a theory paper was published and offered a model to explain the edge states [73]. The calculation shows that when $n > 2$, the strain caused by the interface between inorganic and organic spacers will be relaxed to the edge lattices, causing a large lattice distortion (Fig. 9a). The distortion is large enough to create new localized state with energy much lower than the band gap [73]. However, there is still no experimental confirmation of the lattice distortion on the edge. A related paper was just published and reports the effect of organic spacer on the distortion of inorganic lattice in the surface of monolayer R–P perovskites [74]. Figure 9b–e demonstrates the sensitivity of electronic band structure to the Pb-I lattices and surface lattice relaxation. The edge emission was just confirmed in a very latest work [75].
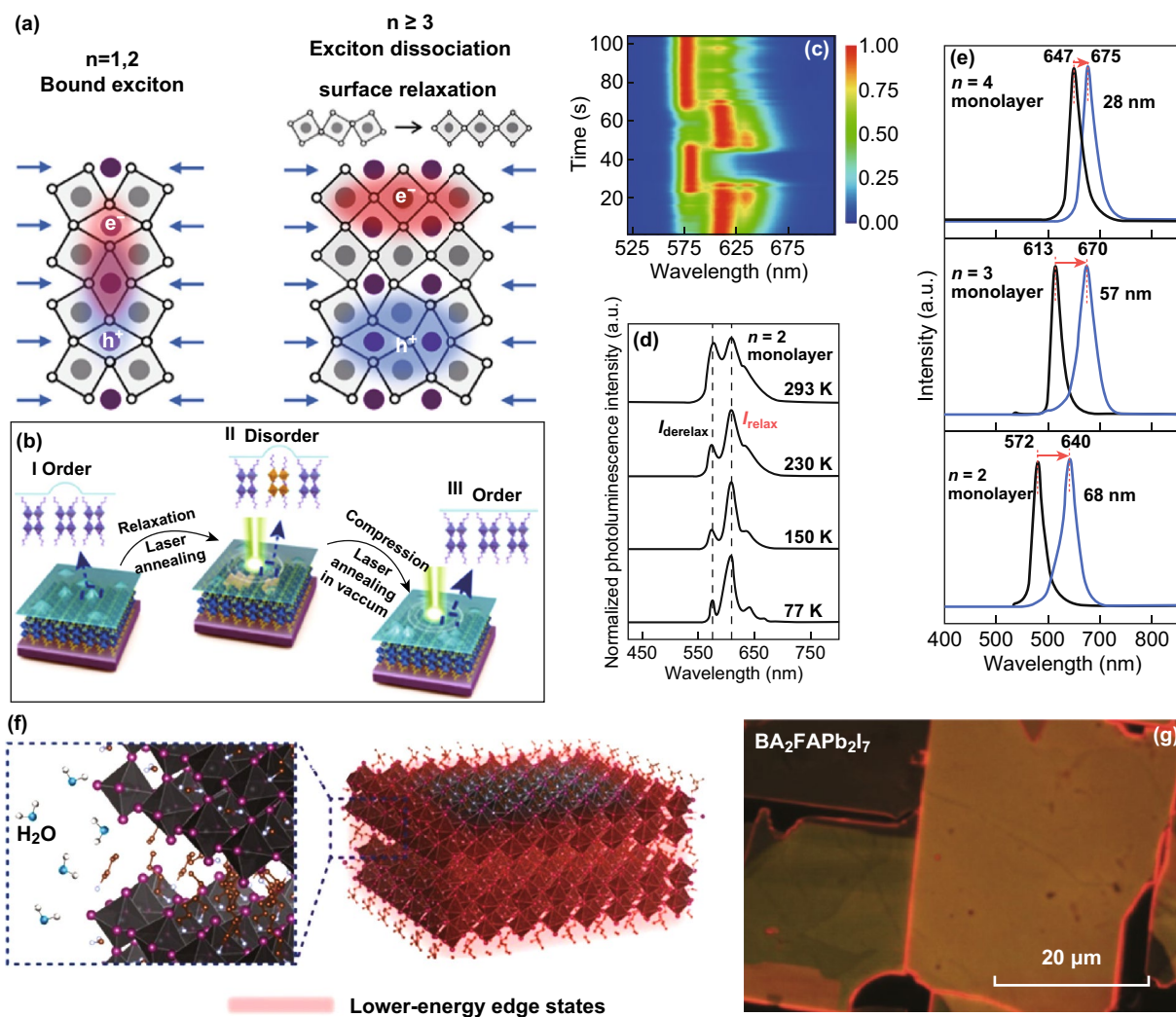

Fig. 9 **a** Schematics of the surface-induced exciton dissociation in R–P perovskites with $n \geq 3$. Reprinted with permission from Ref. [73]. Copyright American Chemical Society. **b** Schematic diagram showing the order–disorder transition by laser illumination. **c** Photoluminescence color map showing two continuous cycles of photoluminescence shifts during order–disorder transition, plotted as a function of laser irradiation time, emission wavelength and intensity. **d** Temperature-dependent changes in photoluminescence intensity. **e** Photoluminescence of $n = 2$–4 R–P perovskite monolayers. Black lines indicate the initial state photoluminescence, and blue lines are photoluminescence after relaxation. Reprinted with permission from Ref. [74]. Copyright Springer Nature. **f** Schematic of edge states of 2D halide perovskite due to moisture. **g** PL image of $BA_2FAPb_2I_7$ excited by UV light. Reprinted with permission from Ref. [75]. Copyright American Chemical Society

But as shown in Fig. 9f–g [75], the edge emission is not due to the intrinsic strain; rather, it is induced by water molecules. Furthermore, the edge emission can also be observed when $n = 2$. Again, these are just experimental observations, and the underlying structure and mechanism are still not clear and require further research.

3 Problems and Challenges in Revealing the Origin of Luminescence Centers in Lead Halide Perovskites

The current problems in identifying the origin of PL from in-gap luminescence centers are due to relatively large inconsistency in the results of both computational simulations and experimental characterization of lead halide perovskites. The basic properties of lead halide perovskites and expected intrinsic point defects have been studied extensively by using DFT. The first attempts of calculating the band structure of lead halide perovskites using local density functionals (LDA) and generalized gradient approximation (GGA) as GGA-PBE produced band gap values in accordance with the experimental ones. The top of valence band in Cs–Pb–Br 0D, 2D and 3D materials is composed of *p*-orbitals of Br with contribution from *s*-orbitals of Pb, whereas the bottom of conduction band is completely based on *p*-orbitals of Pb. Lead is a heavy metal known to possess strong spin–orbital coupling (SOC). The must-have inclusion of SOC in GGA-PBE calculations, however, results in a strong underestimate of band gap values in these materials. This also influences significantly the energy calculations of the native point defects (vacancies, interstitials and antisites) and defect complexes. The energy-level positions of different defects with respect to the band gap edges change with activating SOC. This makes quite dubious the assignment of certain defects as deep in-gap luminescence centers. The analysis of this problem has found its first solution in 2015 when Du [76] showed that the local density functionals used without SOC produce correct band gap values due to error cancelations [77], whereas inclusion of SOC involves self-interacting errors and requires the use of screened hybrid functionals as Heyd–Scuseria–Ernzerhof (HSE) to reproduce correctly both the band gap and the energy position of defects. Kang and Wang [5] presented the first complete calculations of the formation energy of all type point defects in CsPbBr$_3$ using

HSE + SOC. The formation energy of defects was calculated taking into account the Fermi energy and atomic chemical potentials of constituents [78, 79]. Although this work seems to deliver solid results, a few details are alarming and indicate that it may not be the final word on solving problems of modeling defects in lead halide perovskites.

The HSE functional includes a portion of non-local Hartree–Fock (HF) exchange in addition to local GGA-PBE one. The HSE functional partitions the Coulomb operator for a pair of charges into two ranges: short $(SR) = \left[1 - erf(\omega r)\right]/r$ and long $(LR) = erf(\omega r)/r$ that are defined and controlled by the range-separation parameter ω set empirically to 0.15 Bohr^{-1} in the so-called HSE03 [80] version and to 0.11 Bohr^{-1} in the HSE06 version. HSE incorporates 25% SR HF exchange (mixing parameter, $a = 0.25$), no LR HF exchange, 75% SR and full LR PBE exchange, and 100% PBE correlation. Test calculations using HSE03 [80] with $a = 0.25$ and $\omega = 0.15$ Bohr^{-1} have reproduced well the band gap of a large number of semiconductors [81], that is, HSE is believed to be a universal functional. The band gap of CsPbBr$_3$, however, is calculated correctly using HSE + SOC only with HF exchange portion a set to 0.43 [5]. Recent extension of HSE + SOC to calculations of 2D CsPb$_2$Br$_3$ and 3D Cs$_4$PbBr$_6$ shows that there are no universal HSE06 parameters a and ω that produce the band gaps correctly for all Cs–Pb–Br compounds [26]. The band gap of CsPb$_2$B$_5$ and Cs$_4$PbBr$_6$ is calculated to be close to the experimental one for $a = 0.2$ [26], that is, different from both $a = 0.43$ for CsPbBr$_3$ and most importantly different from $a = 0.25$ of the original HSE06 that has been claimed to be a universal for correct calculations of band gaps in semiconductors. One yet unexplored path is to repeat these calculations with fixed original $a = 0.25$ in HSE functional and varying the screen parameter ω and then find a physical reason for different screening parameters in Cs–Pb–Br compounds.

The DFT results of defect formation energy calculations of CsPbBr$_3$, CsPb$_2$Br$_5$ and Cs$_4$PbBr$_6$ and the defect energy levels with respect to the energy band gap in these compounds are shown in Fig. 10 [26]. The defect formation energy was calculated in a similar way as in Ref. [5], but the results for some of the defects in CsPbBr$_3$ are different in the two papers. No critical analysis has been done so far on whether this is the most reliable and realistic approach for calculations of the defect formation energy. Apart
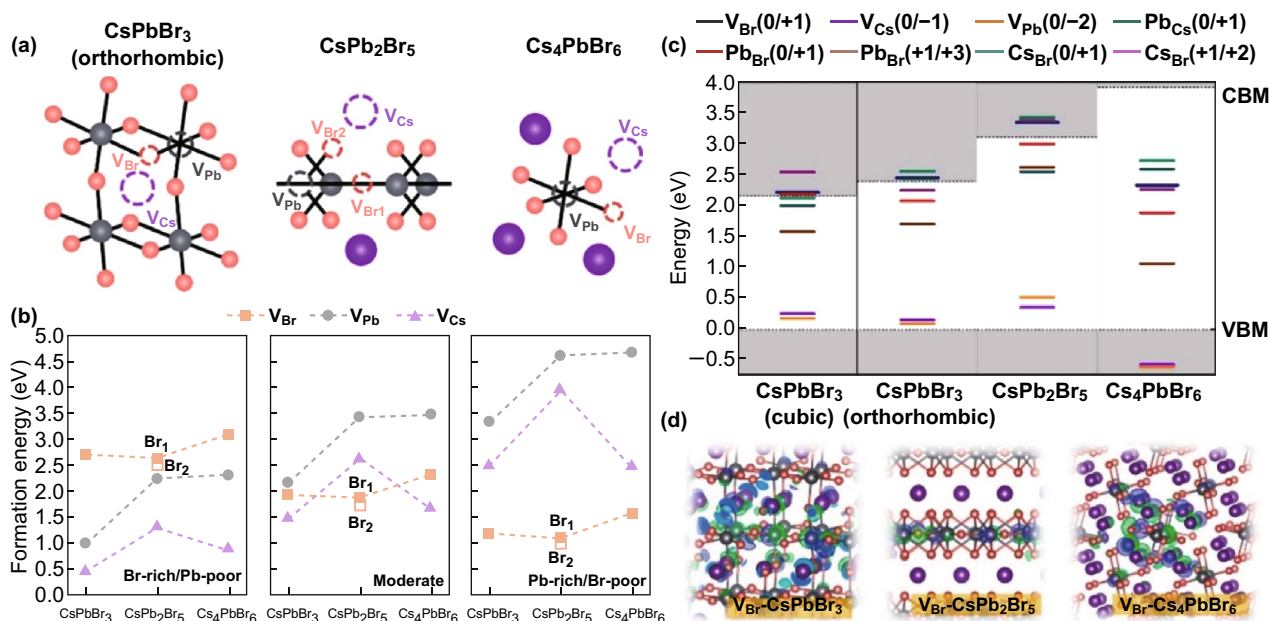
Fig. 10 a Illustrations of Br, Pb and Cs vacancies (VBr, VPb and VCs). **b** Calculated defect formation energies for orthorhombic-$CsPbBr_3$, $CsPb_2Br_5$ and Cs_4PbBr_6 at Br-rich/Pb-poor, moderate and Pb-rich/Br-poor conditions. **c** Defect charge transition levels of $CsPbBr_3$, $CsPb_2Br_5$ and Cs_4PbBr_6. **d** Charge density distributions of V_{Br} defect states for $CsPbBr_3$, $CsPb_2Br_5$ and Cs_4PbBr_6 calculated at the GGA/PBE level of theory. The band gaps were corrected using the HSE + SOC method. Reprinted with permission from Ref. [26]. Copyright American Chemical Society

from the supercell size-independent errors in these calculations as the choice of DFT functional and the choice of exchange correlation potentials discussed above, there are a number of supercell size-dependent errors, e.g., in Ref. [82], that have not been explored yet in the Cs–Pb–Br compounds. There is a need for a more rigorous approach to defect property calculations for the Cs–Pb–Br system in accordance with analyses and prescriptions given in Ref. [83].

The origin of green PL in Cs_4PbBr_6 is attributed to Br vacancies, V_{Br} (as in Ref. [26]). As shown in Fig. 10c, however, V_{Br} (0/+1) cannot be involved in the green PL emission observed in $CsPb_2Br_5$. The only candidates for defect mediated PL in $CsPb_2Br_5$ are the antisites Pb_{Br} and Cs_{Br}. Another computational study of $CsPb_2Br_5$ [33], however, predicts the positions of unoccupied and occupied levels of V_{Br} (0) to lay at ~ 0.25 and ~ 0.5 eV, respectively, below the conduction band edge. The puzzle of the very similar green PL in $CsPb_2Br_5$ and Cs_4PbBr_6 due to defects remains unsolved. These notes show the complexity involved in the

modeling of Cs–Pb–Br compounds and their native point defects and the degree of confidence one may have in the DFT results.

The arguments in favor of green PL in $CsPb_2Br_5$ and Cs_4PbBr_6 due to $CsPbBr_3$ nanocrystal inclusions are better justified experimentally than those in support of native point defects. Indeed, the studies of $CsPbBr_3$ absorption and emission spectra variation with nanocrystal size clearly show a quantum dot size effects with a PL peak position shift from 2.35 eV in bulk crystals to 2.7 eV in ~ 4-nm crystal [28, 84].

The results in Fig. 11 show that typically observed green PL luminescence at 2.35–2.5 eV in $CsPb_2Br_5$ and Cs_4PbBr_6 may well be due to $CsPbBr_3$ nanocrystal inclusions in these wide band gap semiconductors. One way to move forward in revealing the nature of luminescence centers is to provide stronger experimental evidence on the nature of PL centers in Cs–Pb–Br system although this is also challenging as we discuss it below.
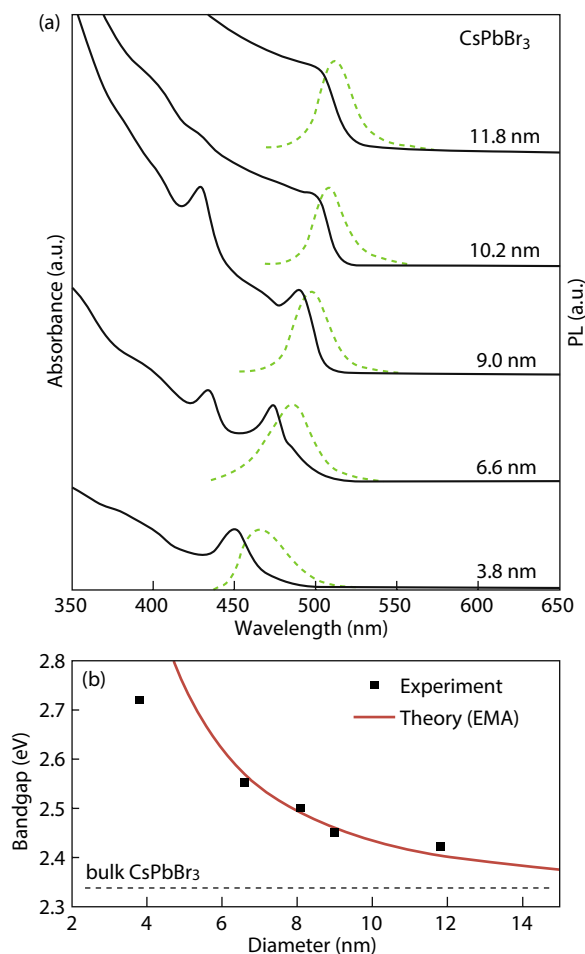
Fig. 11 a Quantum size effects in the absorption and emission spectra of 5–12-nm $CsPbBr_3$ NCs. **b** Experimental versus theoretical (effective mass approximation) size dependence of the band gap energy. Reprinted with permission from Ref. [28]. Copyright American Chemical Society

4 Designing Combined Experimental Characterization Approaches for Better Consistency

Structure–property relation is the major goal of materials science and engineering. Specifically for the Cs–Pb–Br system one of the important properties is the photoluminescence, while its structure is determined by XRD, TEM and Raman spectroscopy. The last one is an indirect structure-related technique. The major reasons for these structure–property controversies or challenges are the difference in probing length scale and sensitivity. XRD is an average technique and has relatively low phase detection sensitivity. It is sensitive to the minority phase domain

size, which below a few hundred nanometers usually diminishes and broadens the related XRD peaks, whereas PL can be emitted even from quantum dots and single molecular inclusions. TEM can provide detailed atomic structures, but there are two major difficulties. The first is that the size of PL and TEM probes are orders of magnitude different. TEM can only probe a much smaller sample, on the order of 100 nm in size; however, micro-PL still require a micrometer-sized sample. The second reason is that perovskite-like materials are very sensitive to electron beams and can get damaged easily, so the structure of perovskite is hard to be studied and advanced low-dose TEM is needed [65].

Raman is a well-established and sensitive technique to identify a material. In addition, Raman is compatible with PL and requires a small sample amount, so Raman can serve both the structure determination and property related to PL. For instance, the non-resonant Raman scattering is structure related, but at resonance it may probe electronic states that concurrently take part in PL. Raman and PL have been separately used in characterizing the luminescent centers, but they were only used for qualitative study, and a combined and calibrated Raman–PL has been missing. The key to such quantitative Raman–PL analysis is the calibrations of both Raman and PL using well-known reference materials. Note that PL is very sensitive to material quality, so a reference sample should be carefully chosen for the combined Raman and PL. For instance, $CsPbBr_3$ nanocrystals can have a PLQY of 60–90% [27–29], but the PLQY of $CsPbBr_3$ micropowders can be as low as 0.1%. $CsPbBr_3$ nanocrystals should be used to confirm whether they are the source for green emission. So far, a successful application of combined Raman/PL mapping of the same sample area of $CsPb_2Br_5$ was reported in Ref. [23]. In that study, the Raman spectroscopy distinguishes the single crystalline part of $CsPb_2Br_5$ [77], which turned out to be non-emissive, from the polycrystalline part that produces green PL.

The optical absorption spectra of Cs–Pb–Br compounds can indicate indirectly, but not for certain, whether the samples are PL emissive or not. A promising alternative approach reported in Ref. [31, 85] uses TEM for structural characterization and energy loss spectroscopy (EELS) in the low-loss region as equivalent of optical absorption in $CsPbBr_3$ and $CsPbBr_3/Cs_4PbBr_6$. The results of TEM–EELS characterization of $CsPbBr_3/Cs_4PbBr_6$ nanocrystals are
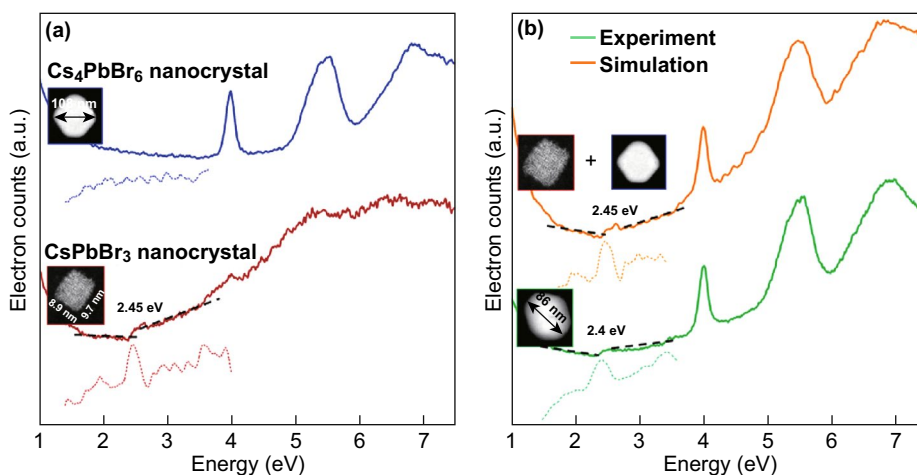
Fig. 12 Energy band gap and structure. **a** Valence-loss EEL spectra representing the absorption of a $CsPbBr_3$ nanocube (red spectrum) and a Cs_4PbBr_6 NC (blue), appearing in the same sample (160 °C). The band gap energy of the nanocube (2.45 eV) is determined from the peak of the first derivative of the EEL spectrum, which appears due to the abrupt onset in absorption (indicated by the dotted lines). No onset is observed for the Cs_4PbBr_6 NC which is an insulator with a large band gap energy of 4 eV. **b** Valence-loss EEL spectrum of a spherical nanocrystal (green) observed in the same sample, formed upon the hybridization of a nanocube and a nanohexagon. The latter process is represented by the simulated EEL spectrum (orange) which is obtained from adding the experimentally obtained spectra of the nanohexagon and nanocube as shown in **a**. The hybrid has, as expected, a band gap energy similar to that of the nanocube. Reprinted with permission from Ref. [31]. Copyright American Chemical Society

shown in Fig. 12. The main limitations of the EELS technique are the effect of sample thickness, relatively low sensitivity and energy resolution in the low-loss region when compared to optical spectroscopy.

The ultimate technique for structure–property relation is combined TEM-PL on a single nanocrystal [86]. The Raman scattering from ultra-small amount of highly luminescence compounds could be too weak to be detectable. A major challenge is to avoid electron beam-induced damages to perovskites. High-resolution TEM imaging has been used by competing sides to support their arguments, but no such combined study was reported. The observation of $CsPbBr_3$/Cs_4PbBr_6 nanocomposites certainly cannot exclude possible defect luminescent states; although no apparent $CsPbBr_3$ nanocrystal was found in some single crystals of emissive Cs_4PbBr_6, PL from the same nanocrystal was actually not demonstrated [19, 51, 55]. More importantly, PL should be performed before and after TEM imaging to ensure no damage has occurred. To reveal the origin of edge states in R–P perovskites [10, 75], the next step is to reproduce the reported results and further determine the factors that are responsible for the edge states. Besides the reported TEM and AFM [75], non-invasive techniques such as Raman and FTIR should be used to identify the structural and chemical changes to the edge lattices [85, 87]. Note that nanometer scale versions of Raman and FTIR are already available to probe local structures [88, 89].

PL, Raman, XRD and TEM are passive techniques; new techniques that can apply external stimulus such as mechanical, electrical, or magnetic force to probe the dynamic response of luminescent centers and distinguish point defect from $CsPbBr_3$ nanocrystals are needed. The challenges and controversies in perovskites have also brought us a great opportunity to test new theory, develop new experimental techniques and eventually provide us new understanding and insight to develop and engineer better materials for a wide range of optoelectronic device applications.

References

1. Y.X. Zhao, K. Zhu, Organic-inorganic hybrid lead halide perovskites for optoelectronic and electronic applications. Chem. Soc. Rev. **45**(3), 655–689 (2016). https://doi.org/10.1039/c4cs00458b

2. J. Huang, Y. Yuan, Y. Shao, Y. Yan, Understanding the physical properties of hybrid perovskites for photovoltaic applications. Nat. Rev. Mater. **2**, 17042 (2017). https://doi.org/10.1038/natrevmats.2017.42

3. J.W. Xiao, L. Liu, D.L. Zhang, N. De Marco, J.W. Lee, O. Lin, Q. Chen, Y. Yang, The emergence of the mixed perovskites and their applications as solar cells. Adv. Energy Mater. **7**, 1700491 (2017). https://doi.org/10.1002/aenm.201700491

4. H.M. Zhu, Y.P. Fu, F. Meng, X.X. Wu, Z.Z. Gong et al., Lead halide perovskite nanowire lasers with low lasing thresholds and high quality factors. Nat. Mater. **14**, 636–642 (2015). https://doi.org/10.1038/nmat4271

5. J. Kang, L.W. Wang, High defect tolerance in lead halide perovskite $CsPbBr_3$. J. Phys. Chem. Lett. **8**, 489–493 (2017). https://doi.org/10.1021/acs.jpclett.6b02800

6. H.R. Lin, C.K. Zhou, Y. Tian, T. Siegrist, B.W. Ma, Low-dimensional organometal halide perovskites. ACS Energy Lett. **3**, 54–62 (2018). https://doi.org/10.1021/acsenergylett.7600926

7. D. Han, C.M. Dai, S.Y. Chen, Calculation studies on point defects in perovskite solar cells. J. Semicond. **38**, 011006 (2017). https://doi.org/10.1088/1674-4926/38/1/011006

8. S. Gonzalez-Carrero, R.E. Galian, J. Perez-Prieto, Organometal halide perovskites: bulk low-dimension materials and nanoparticles. Part. Part. Syst. Charact. **32**, 709–720 (2015). https://doi.org/10.1002/ppsc.201400214

9. K. Hong, Q.V. Le, S.Y. Kim, H.W. Jang, Low-dimensional halide perovskites: review and issues. J. Mater. Chem. C **6**, 2189–2209 (2018). https://doi.org/10.1039/c7tc05658c

10. J.C. Blancon, H. Tsai, W. Nie, C.C. Stoumpos, L. Pedesseau et al., Extremely efficient internal exciton dissociation through edge states in layered 2D perovskites. Science **355**, 1288–1291 (2017). https://doi.org/10.1126/science.aal4211

11. M.I. Saidaminov, J. Almutlaq, S. Sarmah, I. Dursun, A.A. Zhumekenov et al., Pure Cs_4PbBr_6: highly luminescent zero dimensional perovskite solids. ACS Energy Lett. **1**, 840–845 (2016). https://doi.org/10.1021/acsenergylett.6b00396

12. I. Dursun, M.D. Bastiani, B. Turedi, B. Alamer, A. Shkurenko et al., $CsPb_2Br_5$ single crystals: synthesis and characterization. Chemsuschem **10**, 3746–3749 (2017). https://doi.org/10.1002/cssc.201701131

13. Z. Zhang, Y. Zhu, W. Wang, W. Zheng, R. Lin, F. Huang, Growth, characterization and optoelectronic applications of pure-phase large-area $CsPb_2Br_5$ flake single crystals. J. Mater. Chem. C **6**, 446–451 (2018). https://doi.org/10.1039/c7tc04834c

14. J. Li, H.J. Zhang, S. Wang, D.B. Long, M.K. Li et al., Synthesis of all-inorganic $CsPb_2Br_5$ perovskite and determination of its luminescence mechanism. RSC Adv. **7**, 54002–54007 (2017). https://doi.org/10.1039/c7ra10693a

15. Q.A. Akkerman, A.L. Abdelhady, L. Manna, Zero-dimensional cesium lead halides: history, properties, and challenges. J. Phys. Chem. Lett. **9**, 2326–2337 (2018). https://doi.org/10.1021/acs.jpclett.8b00572

16. D. Han, H.L. Shi, W.M. Ming, C.K. Zhou, B.W. Ma et al., Unraveling luminescence mechanisms in zero-dimensional halide perovskites. J. Mater. Chem. C **6**, 6398–6405 (2018). https://doi.org/10.1039/c8tc01291a

17. X.Z. Min, P.C. Zhu, S. Gu, J. Zhu, Research progress of low-dimensional perovskites: synthesis, properties and optoelectronic applications. J. Semicond. **38**, 011004 (2017). https://doi.org/10.1088/1674-4926/38/1/011004

18. R. Guo, Z.A. Zhu, A. Boulesbaa, F. Hao, A. Puretzky et al., Synthesis and photoluminescence properties of 2D phenethylammonium lead bromide perovskite nanocrystals. Small Methods **1**, 1700245 (2017). https://doi.org/10.1002/smtd.201700245

19. K.H. Wang, L. Wu, L. Li, H.B. Yao, H.S. Qian, S.H. Yu, Large-scale synthesis of highly luminescent perovskite-related $CsPb_2Br_5$ nanoplatelets and their fast anion exchange. Angew. Chem. Int. Ed. **55**, 8328–8332 (2016). https://doi.org/10.1002/anie.201602787

20. B. Turedi, K.J. Lee, I. Dursun, B. Alamer, Z.N. Wu et al., Water-induced dimensionality reduction in metal-halide perovskites. J. Phys. Chem. C **122**, 14128–14134 (2018). https://doi.org/10.1021/acs.jpcc.8b01343

21. X.L. Zhang, B. Xu, J.B. Zhang, Y. Gao, Y.J. Zheng, K. Wang, X.W. Sun, All-inorganic perovskite nanocrystals for high-efficiency light emitting diodes: dual-phase $CsPbBr_3$–$CsPb_2Br_5$ composites. Adv. Funct. Mater. **26**, 4595–4600 (2016). https://doi.org/10.1002/adfm.201600958

22. G.P. Li, H. Wang, Z.F. Zhu, Y.J. Chang, T. Zhang, Z.H. Song, Y. Jiang, Shape and phase evolution from $CsPbBr_3$ perovskite nanocubes to tetragonal $CsPb_2Br_5$ nanosheets with an indirect bandgap. Chem. Commun. **52**, 11296–11299 (2016). https://doi.org/10.1039/c6cc05877a

23. Y. Wang, C. Wang, X. Su, V.G. Hadjiev, H.A.C. Benavides et al., Bright luminescent surface states on the edges of wide-bandgap two-dimensional lead halide perovskite. arXiv: 180311490 (2018)

24. K.J.L.B. Turedi, I. Dursun, B. Alamer, Z. Wu, E. Alarousu et al., Water-induced dimensionality reduction in metal-halide perovskites. J. Phys. Chem. C **122**, 14128–14134 (2018). https://doi.org/10.1021/acs.jpcc.8b01343

25. S. Seth, A. Samanta, Photoluminescence of zero-dimensional perovskites and perovskite-related materials. J. Phys. Chem. Lett. **9**, 176–183 (2018). https://doi.org/10.1021/acs.jpclett.7b02931

26. J. Yin, H. Yang, K. Song, A.M. El-Zohry, Y. Han, O.M. Bakr, J.L. Bredas, O.F. Mohammed, Point defects and green

emission in zero-dimensional perovskites. J. Phys. Chem. Lett. **9**, 5490–5495 (2018). https://doi.org/10.1021/acs.jpclett.8b02477

27. J.Z. Song, J.H. Li, X.M. Li, L.M. Xu, Y.H. Dong, H.B. Zeng, Quantum dot light-emitting diodes based on inorganic perovskite cesium lead halides ($CsPbX_3$). Adv. Mater. **27**, 7162 (2015). https://doi.org/10.1002/adma.201502567

28. L. Protesescu, S. Yakunin, M.I. Bodnarchuk, F. Krieg, R. Caputo et al., Nanocrystals of cesium lead halide perovskites ($CsPbX_3$, $X = Cl$, Br, and I): novel optoelectronic materials showing bright emission with wide color gamut. Nano Lett. **15**, 3692–3696 (2015). https://doi.org/10.1021/nl5048779

29. H.C. Wang, S.Y. Lin, A.C. Tang, B.P. Singh, H.C. Tong et al., Mesoporous silica particles integrated with all-inorganic $CsPbBr_3$ perovskite quantum-dot nanocomposites (MP-PQDs) with high stability and wide color gamut used for backlight display. Angew. Chem. Int. Ed. **55**, 7924–7929 (2016). https://doi.org/10.1002/anie.201603698

30. Z.K. Liu, Y. Bekenstein, X.C. Ye, S.C. Nguyen, J. Swabeck et al., Ligand mediated transformation of cesium lead bromide perovskite nanocrystals to lead depleted Cs_4PbBr_6 nanocrystals. J. Am. Chem. Soc. **139**, 5309–5312 (2017). https://doi.org/10.1021/jacs.7b01409

31. C. de Weerd, J.H. Lin, L. Gomez, Y. Fujiwara, K. Suenaga, T. Gregorkiewicz, Hybridization of single nanocrystals of Cs_4PbBr_6 and $CsPbBr_3$. J. Phys. Chem. C **121**, 19490–19496 (2017). https://doi.org/10.1021/acs.jpcc.7b05752

32. L. Yang, D.M. Li, C. Wang, W. Yao, H. Wang, K.X. Huang, Room-temperature synthesis of pure perovskite-related Cs_4PbBr_6 nanocrystals and their ligand-mediated evolution into highly luminescent $CsPbBr_3$ nanosheets. J. Nanopart. Res. **19**, 258 (2017). https://doi.org/10.1007/s11051-017-3959-7

33. F. Iyikanat, E. Sari, H. Sahin, Thinning $CsPb_2Br_5$ perovskite down to monolayers: Cs-dependent stability. Phys. Rev. B **96**, 155442 (2017). https://doi.org/10.1103/PhysRevB.96.155442

34. J.W. Xu, W.X. Huang, P.Y. Li, D.R. Onken, C.C. Dun et al., Imbedded nanocrystals of $CsPbBr_3$ in Cs_4PbBr_6: kinetics, enhanced oscillator strength, and application in light-emitting. Adv. Mater. **29**, 1703703 (2017). https://doi.org/10.1002/adma.1703703

35. Y. Bekenstein, B.A. Koscher, S.W. Eaton, P.D. Yang, A.P. Alivisatos, Highly luminescent colloidal nanoplates of perovskite cesium lead halide and their oriented assemblies. J. Am. Chem. Soc. **137**, 16008–16011 (2015). https://doi.org/10.1021/jacs.5b11199

36. D.D. Zhang, S.W. Eaton, Y. Yu, L.T. Dou, P.D. Yang, Solution-phase synthesis of cesium lead halide perovskite nanowires. J. Am. Chem. Soc. **137**, 9230–9233 (2015). https://doi.org/10.1021/jacs.5b05404

37. C.K. Zhou, Y. Tian, M.C. Wang, A. Rose, T. Besara et al., Low-dimensional organic tin bromide perovskites and their photoinduced structural transformation. Angew. Chem. Int. Ed. **56**, 9018–9022 (2017). https://doi.org/10.1002/anie.201702825

38. H.L.C. Zhou, Q. He, L. Xu, M. Worku, M. Chaaban et al., Low dimensional metal halide perovskites and hybrids. Mater.

Sci. Eng. **R137**, 38–65 (2019). https://doi.org/10.1016/j.mser.2018.12.001

39. P. Zhang, G.D. Zhang, L. Liu, D.X. Ju, L.Z. Zhang, K. Cheng, X.T. Tao, Anisotropic optoelectronic properties of melt-grown bulk $CsPbBr_3$ single crystal. J. Phys. Chem. Lett. **9**, 5040–5046 (2018). https://doi.org/10.1021/acs.jpclett.8b01945

40. M.Z. Zhang, Z.P. Zheng, Q.Y. Fu, P.J. Guo, S. Zhang et al., Determination of defect levels in melt-grown all-inorganic perovskite $CsPbBr_3$ crystals by thermally stimulated current spectra. J. Phys. Chem. C **122**, 10309–10315 (2018). https://doi.org/10.1021/acs.jpcc.8b01532

41. M. Rodova, J. Brozek, K. Knizek, K. Nitsch, Phase transitions in ternary caesium lead bromide. J. Therm. Anal. Calorim. **71**, 667–673 (2003). https://doi.org/10.1023/a:1022836800820

42. F.J. Ye, W.Q. Yang, D.Y. Luo, R. Zhu, Q.H. Gong, Applications of cesium in the perovskite solar cells. J. Semicond. **38**, 011003 (2017). https://doi.org/10.1088/1674-4926/38/1/011003

43. Q.S. Sun, C.L. Ni, Y.C. Yu, S. Attique, S.Y. Wei et al., Design principle of all-inorganic halide perovskite-related nanocrystals. J. Mater. Chem. C **6**, 12484–12492 (2018). https://doi.org/10.1039/c8tc04254c

44. Z.J. Zhang, Y.M. Zhu, W.L. Wang, W. Zheng, R.C. Lin et al., Aqueous solution growth of millimeter-sized nongreen-luminescent wide bandgap Cs_4PbBr_6 bulk crystal. Cryst. Growth Des. **18**, 6393–6398 (2018). https://doi.org/10.1021/acs.cgd.8b00817

45. W. Shen, L.F. Ruan, Z.T. Shen, Z.T. Deng, Reversible light-mediated compositional and structural transitions between $CsPbBr_3$ and $CsPb_2Br_5$ nanosheets. Chem. Commun. **54**, 2804–2807 (2018). https://doi.org/10.1039/c8cc00139a

46. M. Cola, V. Massarot, R. Riccardi, C. Sinistri, Binary systems formed by lead bromide with (Li, Na, K, Rb, Cs and Tl)Br: a DTA and diffractometric study. Zeitschrift für Naturforschung A **A 26**(8), 1328–1332 (1971). https://doi.org/10.1515/zna-1971-0812

47. X.S. Tang, Z.P. Hu, W. Yuan, W. Hu, H.B. Shao et al., Perovskite $CsPb_2Br_5$ microplate laser with enhanced stability and tunable properties. Adv. Opt. Mater. **5**, 1600788 (2017). https://doi.org/10.1002/adom.201600788

48. L. Ruan, W. Shen, A. Wang, A. Xiang, Z. Deng, Alkyl-thiol ligands induced shape and crystalline phase controlled synthesis of stable perovskite-related $CsPb_2Br_5$ nanocrystals at room temperature. J. Phys. Chem. Lett. **8**, 3853–3860 (2017). https://doi.org/10.1021/acs.jpclett.7b01657

49. P.Z. Li, C.B. Hu, L. Zhou, J.T. Jiang, Y.Z. Cheng, M.L. He, X.J. Liang, W.D. Xiang, Novel synthesis and optical characterization of $CsPb_2Br_5$ quantum dots in borosilicate glasses. Mater. Lett. **209**, 483–485 (2017). https://doi.org/10.1016/j.matlet.2017.08.079

50. C.J. Qin, T. Matsushima, A.S.D. Sandanayaka, Y. Tsuchiya, C. Adachi, Centrifugal-coated quasi-two-dimensional perovskite $CsPb_2Br_5$ films for efficient and stable light-emitting diodes. J. Phys. Chem. Lett. **8**, 5415–5421 (2017). https://doi.org/10.1021/acs.jpclett.7b02371

51. J.F. Lv, L.L. Fang, J.Q. Shen, Synthesis of highly luminescent $CsPb_2Br_5$ nanoplatelets and their application for

light-emitting diodes. Mater. Lett. **211**, 199–202 (2018). https://doi.org/10.1016/j.matlet.2017.09.106

52. C. Han, C.L. Li, Z.G. Zang, M. Wang, K. Sun, X.S. Tang, J.H. Du, Tunable luminescent $CsPb_2Br_5$ nanoplatelets: applications in light-emitting diodes and photodetectors. Photonics Res. **5**, 473–480 (2017). https://doi.org/10.1364/prj.5.000473

53. P.Z. Li, Y.Z. Cheng, L. Zhou, X.Q. Yu, J.T. Jiang, M.L. He, X.J. Liang, W.D. Xiang, Photoluminescence properties and device application dots in glasses of $CsPb_2Br_5$ quantum dots in glasses. Mater. Res. Bull. **105**, 63–67 (2018). https://doi.org/10.1016/j.materresbull.2018.04.028

54. K.W. Wu, A. Bera, C. Ma, Y.M. Du, Y. Yang, L. Li, T. Wu, Temperature-dependent excitonic photoluminescence of hybrid organometal halide perovskite films. Phys. Chem. Chem. Phys. **16**, 22476–22481 (2014). https://doi.org/10.1039/c4cp03573a

55. L.F. Ruan, J. Lin, W. Shen, Z.T. Deng, Ligand-mediated synthesis of compositionally related cesium lead halide $CsPb_2X_5$ nanowires with improved stability. Nanoscale **10**, 7658–7665 (2018). https://doi.org/10.1039/c8nr00883c

56. F. Palazon, S. Dogan, S. Marras, F. Locardi, I. Nelli et al., From $CsPbBr_3$ nano-inks to sintered $CsPbBr_3$–$CsPb_2Br_5$ films via thermal annealing: implications on optoelectronic properties. J. Phys. Chem. C **121**, 11956–11961 (2017). https://doi.org/10.1021/acs.jpcc.7b03389

57. B. Qiao, P.J. Song, J.Y. Cao, S.L. Zhao, Z.H. Shen et al., Water-resistant, monodispersed and stably luminescent $CsPbBr_3/CsPb_2Br_5$ core-shell-like structure lead halide perovskite nanocrystals. Nanotechnology **28**, 445602 (2017). https://doi.org/10.1088/1361-6528/aa892e

58. S.K. Balakrishnan, P.V. Kamat, Ligand assisted transformation of cubic $CsPbBr_3$ nanocrystals into two-dimensional $CsPb_2Br_5$ nanosheets. Chem. Mater. **30**, 74–78 (2017). https://doi.org/10.1021/acs.chemmater.7b04142

59. C.K. Zhou, Y. Tian, Z. Yuan, H.R. Lin, B.H. Chen et al., Highly efficient broadband yellow phosphor based on zero-dimensional tin mixed-halide perovskite. ACS Appl. Mater. Interfaces **9**, 44579–44583 (2017). https://doi.org/10.1021/acsami.7b12862

60. C.K. Zhou, H.R. Lin, Y. Tian, Z. Yuan, R. Clark et al., Luminescent zero-dimensional organic metal halide hybrids with near-unity quantum efficiency. Chem. Sci. **9**, 586–593 (2018). https://doi.org/10.1039/c7sc04539e

61. J. Yin, P. Maity, M. De Bastiani, I. Dursun, O.M. Bakr, J.L. Bredas, O.F. Mohammed, Molecular behavior of zero-dimensional perovskites. Sci. Adv. **3**, e1701793 (2017). https://doi.org/10.1126/sciadv.1701793

62. J. Yin, Y.H. Zhang, A. Bruno, C. Soci, O.M. Bakr, J.L. Bredas, O.F. Mohammed, Intrinsic lead ion emissions in zero-dimensional Cs_4PbBr_6 nanocrystals. ACS Energy Lett. **2**, 2805–2811 (2017). https://doi.org/10.1021/acsenergylett.7b01026

63. M. De Bastiani, I. Dursun, Y.H. Zhang, B.A. Alshankiti, X.H. Miao et al., Inside perovskites: quantum luminescence from bulk Cs_4PbBr_6 single crystals. Chem. Mater. **29**, 7108–7113 (2017). https://doi.org/10.1021/acs.chemmater.7b02415

64. J. Almutlaq, J. Yin, O.F. Mohammed, O.M. Bakr, The benefit and challenges of zero-dimensional perovskites. J. Phys. Chem. Lett. **9**, 4131–4138 (2018). https://doi.org/10.1021/acs.jpclett.8b00532

65. Y. Zhang, L. Sinatra, E. Alarousu, J. Yin, A.M. El-Zohry, O.M. Bakr, O.F. Mohammed, Ligand-free nanocrystals of highly emissive Cs_4PbBr_6 perovskite. J. Phys. Chem. C **122**, 6493–6498 (2018). https://doi.org/10.1021/acs.jpcc.8b01735

66. J.H. Cha, J.H. Han, W. Yin, C. Park, Y. Park et al., Photoresponse of $CsPbBr_3$ and Cs_4PbBr_6 perovskite single crystals. J. Phys. Chem. Lett. **8**, 565–570 (2017). https://doi.org/10.1021/acs.jpclett.6b02763

67. D.Q. Chen, Z.Y. Wan, X. Chen, Y.J. Yuan, J.S. Zhong, Large-scale room-temperature synthesis and optical properties of perovskite-related Cs_4PbBr_6 fluorophores. J. Mater. Chem. C **4**, 10646–10653 (2016). https://doi.org/10.1039/c6tc04036e

68. S. Seth, A. Samanta, Fluorescent phase-pure zero-dimensional perovskite-related Cs_4PbBr_6 microdisks: synthesis and single-particle imaging study. J. Phys. Chem. Lett. **8**, 4461–4467 (2017). https://doi.org/10.1021/acs.jpclett.7b02100

69. Z.J. Zhang, W. Zheng, R.C. Lin, F. Huang, One-step on-chip synthesis of highly-luminescent Cs_4PbBr_6 microcrystal. Mater. Lett. **232**, 118–121 (2018). https://doi.org/10.1016/j.matlet.2018.08.083

70. W.K. Wang, D.F. Wang, F. Fang, S. Wang, G.H. Xu, T.J. Zhang, $CsPbBr_3/Cs_4PbBr_6$ nanocomposites: formation mechanism, large-scale and green synthesis, and application in white light-emitting diodes. Cryst. Growth Des. **18**, 6133–6141 (2018). https://doi.org/10.1021/acs.cgd.8b01013

71. Q.A. Akkerman, S. Park, E. Radicchi, F. Nunzi, E. Mosconi et al., Nearly monodisperse insulator Cs_4PbX_6 ($X = Cl$, Br, I) nanocrystals, their mixed halide compositions, and their transformation into $CsPbX_3$ nanocrystals. Nano Lett. **17**, 1924–1930 (2017). https://doi.org/10.1021/acs.nanolett.6b05262

72. X.M. Chen, F. Zhang, Y. Ge, L.F. Shi, S. Huang et al., Centimeter-sized Cs_4PbBr_6 crystals with embedded $CsPbBr_3$ nanocrystals showing superior photoluminescence: nonstoichiometry induced transformation and light-emitting applications. Adv. Funct. Mater. **28**, 1706567 (2018). https://doi.org/10.1002/adfm.201706567

73. M. Kepenekian, B. Traore, J.C. Blancon, L. Pedesseau, H. Tsai et al., Concept of lattice mismatch and emergence of surface states in two-dimensional hybrid perovskite quantum wells. Nano Lett. **18**, 5603–5609 (2018). https://doi.org/10.1021/acs.nanolett.8b02078

74. K. Leng, I. Abdelwahab, I. Verzhbitskiy, M. Telychko, L.Q. Chu et al., Molecularly thin two-dimensional hybrid perovskites with tunable optoelectronic properties due to reversible surface relaxation. Nat. Mater. **17**, 908 (2018). https://doi.org/10.1038/s41563-018-0164-8

75. E. Shi, S. Deng, B. Yuan, Y. Gao, Akriti et al., Extrinsic and dynamic edge states of two-dimensional lead halide perovskites. ACS Nano (2019). https://doi.org/10.1021/acsnano.8b07631

76. M.H. Du, Density functional calculations of native defects in $CH_3NH_3PbI_3$: effects of spin-orbit coupling and

self-interaction error. J. Phys. Chem. Lett. **6**, 1461–1466 (2015). https://doi.org/10.1021/acs.jpclett.5b00199

77. E. Mosconi, A. Amat, M.K. Nazeeruddin, M. Gratzel, F. De Angelis, First-principles modeling of mixed halide organometal perovskites for photovoltaic applications. J. Phys. Chem. C **117**, 13902–13913 (2013). https://doi.org/10.1021/jp4048659

78. S.B. Zhang, S.H. Wei, Nitrogen solubility and induced defect complexes in epitaxial GaAs: N. Phys. Rev. Lett. **86**, 1789–1792 (2001). https://doi.org/10.1103/PhysRevLett.86.1789

79. S.H. Wei, S.B. Zhang, Chemical trends of defect formation and doping limit in II–VI semiconductors: the case of CdTe. Phys. Rev. B **66**, 155211 (2002). https://doi.org/10.1103/PhysRevB.66.155211

80. J. Heyd, G.E. Scuseria, M. Ernzerhof, Hybrid functionals based on a screened Coulomb potential. J. Chem. Phys. **118**, 8207–8215 (2003). https://doi.org/10.1063/1.1564060

81. J. Heyd, J.E. Peralta, G.E. Scuseria, R.L. Martin, Energy band gaps and lattice parameters evaluated with the Heyd–Scuseria–Ernzerhof screened hybrid functional. J. Chem. Phys. **123**, 174101 (2005). https://doi.org/10.1063/1.2085170

82. C.W.M. Castleton, A. Hoglund, S. Mirbt, Density functional theory calculations of defect energies using supercells. Model. Simul. Mater. Sci. Eng. **17**, 084003 (2009). https://doi.org/10.1088/0965-0393/17/8/084003

83. C. Freysoldt, B. Grabowski, T. Hickel, J. Neugebauer, G. Kresse, A. Janotti, C.G. Van de Walle, First-principles calculations for point defects in solids. Rev. Mod. Phys. **86**, 253 (2014). https://doi.org/10.1103/RevModPhys.86.253

84. M.C. Brennan, J.E. Herr, T.S. Nguyen-Beck, J. Zinna, S. Draguta, S. Rouvimov, J. Parkhill, M. Kuno, Origin of the size-dependent stokes shift in CsPbBr$_3$ perovskite nanocrystals. J. Am. Chem. Soc. **139**, 12201–12208 (2017). https://doi.org/10.1021/jacs.7b05683

85. V.G. Hadjiev, C. Wang, Y. Wang, X. Su, H.A. Calderon et al., Phonon fingerprints of CsPb$_2$Br$_5$. J. Phys.: Condes. Matter **30**, 405703 (2018). https://doi.org/10.1088/1361-648X/aadeb4

86. J.M. Bao, D.C. Bell, F. Capasso, J.B. Wagner, T. Martensson, J. Tragardh, L. Samuelson, Optical properties of rotationally twinned InP nanowire heterostructures. Nano Lett. **8**, 836–841 (2008). https://doi.org/10.1021/nl072921e

87. Z. Zhu, V.G. Hadjiev, Y.G. Rong, R. Guo, B. Cao et al., Interaction of organic cation with water molecule in perovskite MAPbI$_3$: from dynamic orientational disorder to hydrogen bonding. Chem. Mater. **28**, 7385–7393 (2016). https://doi.org/10.1021/acs.chemmater.6b02883

88. A. Dazzi, C.B. Prater, AFM-IR: Technology and applications in nanoscale infrared spectroscopy and chemical imaging. Chem. Rev. **117**, 5146–5173 (2017). https://doi.org/10.1021/acs.chemrev.6b00448

89. G. Kolhatkar, J. Plathier, A. Ruediger, Nanoscale investigation of materials, chemical reactions, and biological systems by tip enhanced Raman spectroscopy—a review. J. Mater. Chem. C **6**, 1307–1319 (2018). https://doi.org/10.1039/c7tc05688e